Observation of intra- and inter-band transitions in the transient optical response of graphene

2013 New J. Phys. 15 015009

(http://iopscience.iop.org/1367-2630/15/1/015009)

New Journal of Physics
The open access journal for physics

Observation of intra- and inter-band transitions in the transient optical response of graphene

Leandro M Malard[1], Kin Fai Mak[1], A H Castro Neto[2,3], N M R Peres[4] and Tony F Heinz[1,5]

[1] Departments of Physics and Electrical Engineering, Columbia University, 538 West 120th Street, New York, NY 10027, USA
[2] Department of Physics, Boston University, 590 Commonwealth Avenue, Boston, MA 02215, USA
[3] Graphene Research Centre, National University of Singapore, 2 Science Drive 3, 117542 Singapore, Singapore
[4] Departamento de Física e Centro de Física, Universidade do Minho, P-4710-057 Braga, Portugal
E-mail: tfh3@columbia.edu

New Journal of Physics **15** (2013) 015009 (14pp)
Received 30 June 2012
Published 22 January 2013
Online at http://www.njp.org/
doi:10.1088/1367-2630/15/1/015009

Abstract. The transient optical conductivity of freely suspended graphene was examined by femtosecond time-resolved spectroscopy using pump excitation at 400 nm and probe radiation at 800 nm. The optical conductivity (or, equivalently, absorption) changes abruptly upon excitation and subsequently relaxes to its initial value on the time scale of 1 ps. The form of the induced change in the optical conductivity varies strongly with excitation conditions, exhibiting a crossover from enhanced to decreased optical conductivity with increasing pump fluence. We describe the graphene response in terms of transient heating of the electrons, with the characteristic relaxation time of the transient conductivity reflecting the cooling of the electron system and the strongly coupled optical phonons through emission of lower energy phonons. The change in the optical conductivity is attributed to a combination of induced absorption from intra-band transitions of the photo-generated carriers and bleaching of the inter-band transitions by Pauli blocking. The former effect, which corresponds to the

[5] Author to whom any correspondence should be addressed.

high-frequency wing of the Drude response, dominates at low pump fluence. In this regime of a limited rise in the electron temperature, an increase in the optical conductivity is observed. At high pump fluence, elevated electron temperatures are achieved. The decrease in the inter-band bleaching then dominates the transient response, the intra-band contribution being overwhelmed despite an increase in the Drude scattering rate with temperature. The temporal evolution of the optical conductivity in all the regimes can be described within a model including the intra- and inter-band contributions with a time-varying electronic temperature. An increased Drude scattering rate is inferred for high electron temperature and mechanisms for this enhancement are considered. The calculated scattering rate for interactions of the carriers with zone-center and zone-edge optical phonons agrees well with the rates obtained from experiment.

Contents

1. Introduction

The optical properties of graphene have been the subject of much recent attention [1–3]. Interest in this topic is generated both by the insight that the optical response of graphene provides into the nature of its excited states and their interactions, and by the importance of understanding graphene's optical response for emerging photonic and optoelectronic applications [2, 4–10]. The response of graphene to excitation by femtosecond laser pulses has attracted particular interest [11–17]. Dynamics on the femtosecond time scale provides information about electron–electron, electron–phonon and phonon–phonon interactions. It also has implications for the behavior of recently developed ultrafast photonic and optoelectronic devices [2, 4–10].

The optical response of graphene can be divided into two fundamental processes: inter-band and intra-band optical transitions [3, 18–20]. Inter-band transitions dominate the absorption channel in the mid-/near-infrared and visible spectral range. The corresponding graphene sheet conductivity for photons that leads to excitations of the graphene band structure in the region of linear dispersion is given by the frequency-independent universal constant of $\pi e^2/2h$ [20, 21]. Whereas the inter-band transitions have been extensively characterized, the influence of intra-band transitions, i.e. of the free carrier absorption, on the transient optical response of graphene in the visible is yet to be established. At longer probe wavelengths, the influence of intra-band transitions becomes stronger, and the role of these transitions in the transient response of photoexcited graphene in the mid-infrared and THz spectral range has

recently been reported [22, 23]. A full understanding of this dynamical response is important for applications of graphene in ultrafast photonic devices, as in saturable absorbers. The free-carrier optical response, we note, is the high-frequency analogue of the much-studied dc transport properties of the material and gives rise to a Drude peak in the far infrared [24]. Although peaked at zero frequency, this response is expected to have a tail that extends into the visible spectral range. Here we report the observation of a *dominant intra-band* contribution to the transient optical response, with a corresponding *enhanced absorption.* We identify this effect through probing freely suspended graphene samples at relatively low pump fluence, complementary to a previous study of the effect of doped epitaxial graphene in the infrared range [14]. With increasing pump fluence, the transient optical response exhibits a crossover from enhanced absorption to bleaching, as Pauli blocking of inter-band transitions becomes more prominent.

We explain the observed temporal evolution of the optical absorption for all pump fluences within the framework of thermalized charge carriers that are in equilibrium with a set of strongly coupled optical phonons (SCOPs), but are out of equilibrium with other graphene phonons. Cooling of this subsystem is understood to be controlled by energy loss of these SCOPs to lower energy phonons through anharmonic decay. A fluence-independent time constant of 1.4 ps for the cooling process is deduced, which is consistent with recent time-resolved Raman scattering measurements of the cooling of zone-center optical phonons [25]. In addition to the importance of these measurements for understanding ultrafast carrier dynamics and applications in ultrafast photonics, the intra-band response observed in these experiments at elevated electron temperature provides insight into carrier dynamics in a regime relevant to high-field charge transport in graphene [26–29]. In particular, our experiments reveal a sharp increase in the Drude scattering rate with increasing temperature of the electrons and optical phonons, as also suggested by high-field electrical transport measurements in carbon nanotubes [30, 31] and graphene [26–29]. Through an explicit calculation, we show that our results are compatible with the behavior expected if electron–optical phonon scattering plays a dominant role in determining the carrier scattering rate in this high-temperature regime.

2. Experiment

In our experimental study, we made use of freely suspended graphene samples. Such samples allow us to eliminate both accidental doping effects and energy transfer associated with the substrate and we can probe the relaxation dynamics without these complications. These effects can alter the intrinsic electron dynamics by introducing extra decay channels, which may account for the variation in relaxation times reported in the literature [13–15]. We prepared exfoliated graphene samples that were freely suspended over trenches patterned in transparent SiO_2 substrates [32]. The substrates, with trenches of widths of 4–5 μm and depths of $\sim$3 μm (as characterized by atomic-force microscopy), were carefully cleaned by chemical etching (nanostrip) before we deposited graphene by mechanical exfoliation from kish graphite. Areas of graphene of single-layer thickness were identified by optical microscopy and further characterized by Raman spectroscopy [32]. The low doping level of the samples was reflected in the large ($\sim$15 cm^{-1}) width of the G-mode, whereas the low level of defects was implied by the absence of the disorder-induced D-mode. We have also characterized the optical absorption spectra of the graphene samples, which were the same as those given in [20, 33].

The optical pump–probe measurements were made using a mode-locked Ti-sapphire laser producing pulses of $\sim$100 fs duration at an 80 MHz repetition rate. The 800 nm wavelength

output of the laser provided the probe pulses, whereas radiation at 400 nm, obtained by frequency doubling in a β-barium borate crystal, served as the pump excitation. Both the pump and probe beams were focused onto the samples with a single 40× objective to yield Gaussian spots of comparable widths of $\sim$1.5 μm (full-width at half-maximum). The pump fluence was varied by using a continuously tunable neutral density filter to guarantee that the alignment of the laser beam remained unchanged. We explicitly checked that the pump–probe time delay, laser pulse duration and spot size were not modified by changing the attenuation. The absorbed pump fluence was determined using the absorbance of graphene at 400 nm ($1.8\pi\alpha = 4.14\%$ [33]). To account for the spatial variation of the pump and probe beams, the effective fluence was determined by weighting the absorbed pump fluence using the spatial profile of the probe beam. Effective absorbed fluences F between 0.5 and 4.0 μJ cm^{-2} were investigated experimentally. We note that over this range of pump fluences, saturation of absorbance in graphene at the pump wavelength is negligible [5].

We made the pump–probe measurements by modulating the pump laser at 20 kHz and detecting the synchronous change in probe transmission. The induced modulation of the probe beam for the lowest pump fluence was $\sim 10^{-6}$. For a suspended thin film of material such as our graphene sample, the fractional decrease in the transmittance, $-\Delta T/T$, is given by the change in the sample absorbance, ΔA. The latter can be directly related to the change in the real part of the optical sheet conductivity of graphene, $\sigma^{(1)}$, according to $\Delta A = (4\pi/c)\Delta\sigma^{(1)}$ [20]. We can therefore directly convert our experimentally observed change in transmission into a fundamental material property of graphene, namely $\Delta\sigma^{(1)}$.

3. Results and discussion

3.1. Experimental results and origin of the transient response

Figure 1(a) shows the measured transient response of graphene for a comparatively low absorbed pump fluence of $F = 0.5\ \mu$J cm^{-2}. An increase in the optical conductivity (enhanced absorption) is seen. The rise time of this response is comparable with our experimental time resolution, whereas the relaxation can be fit to a single exponential decay with a time constant of $\tau_{\rm exp} = 3.1$ ps.

To analyze our data, we consider models for the optical conductivity of graphene with the electronic system described by a Fermi–Dirac distribution at (electronic) temperature T. The assumption of a thermalized energy distribution for the electronic excitations is justified by the time resolution of >100 fs in our measurements. On this time scale, the excited electrons and holes are expected to be equilibrated with one another, as well with the SCOPs near the Γ- and K-points [11, 34]. These SCOPs are the set of in-plane optical phonons for which intra- and inter-valley carrier scattering can simultaneously conserve energy and momentum [35]. We note that the electron–electron interactions are expected to be strong and lead to the existence of a thermalized electron energy distribution on the time scale relevant for these measurements [16, 36].

The predicted change in the optical conductivity of graphene under excitation arises from both intra- and inter-band contributions, $\Delta\sigma^{(1)} = \Delta\sigma^{(1)}_{\rm intra} + \Delta\sigma^{(1)}_{\rm inter}$. For the case of thermalized electronic energy distributions relevant to our case, the optical response of graphene has been examined in several theoretical investigations [3, 18, 19]. Within a picture of non-interacting electrons, the induced change in the real part of the optical sheet conductivity follows directly

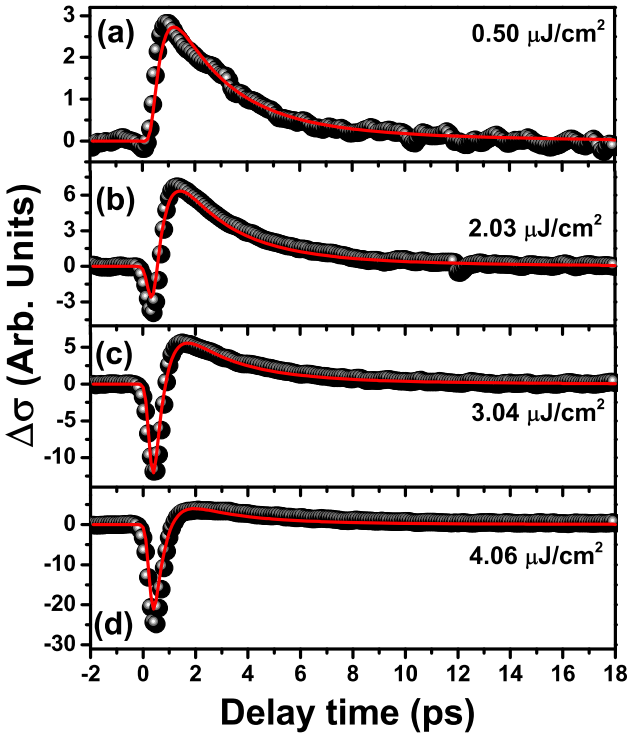

Figure 1. Measured transient optical conductivity of graphene (dots) for the excitation of different absorbed pump fluences F: (a) $0.50\,\mu\mathrm{J\,cm^{-2}}$, (b) $2.03\,\mu\mathrm{J\,cm^{-2}}$, (c) $3.04\,\mu\mathrm{J\,cm^{-2}}$ and (d) $4.06\,\mu\mathrm{J\,cm^{-2}}$. The red curves are fits based on the model described in the text, which include both intra- and inter-band contributions to the optical response.

from the corresponding changes in the intra- and inter-band terms:

$$\sigma^{(1)}_{\mathrm{intra}} = \frac{8\ln 2}{\pi}\frac{\pi e^2}{2h}\frac{\Gamma k_{\mathrm{B}}T}{(\hbar\omega)^2+\Gamma^2},$$
$$\sigma^{(1)}_{\mathrm{inter}} = \frac{\pi e^2}{2h}\tanh\left(\frac{\hbar\omega}{4k_{\mathrm{B}}T}\right). \tag{1}$$

Here $\hbar\omega$ denotes the photon energy of the probe beam, and Γ is the scattering rate (in units of energy). For our suspended graphene samples, we have negligible doping and have taken the chemical potential to lie at the Dirac point. We also neglect any transient separation of the chemical potentials for the electrons and holes. While a dynamical separation of the chemical potentials is common in semiconductors under ultrafast excitation, on the relevant time scale the effect is expected to be insignificant in graphene because of the presence of rapid Auger processes for this zero-gap material [5, 17]. We note that this treatment neglects many-body effects. We do not expect these corrections to alter the key features of the dynamics discussed here. Also neglected in this formulation is the influence of dephasing and the associated spectral broadening for the inter-band transitions.

The photo-induced change in the optical conductivity in equation (1) from intra-band transitions, $\Delta\sigma^{(1)}_{\mathrm{intra}}$, is expected to be positive in sign. The enhanced conductivity arises from

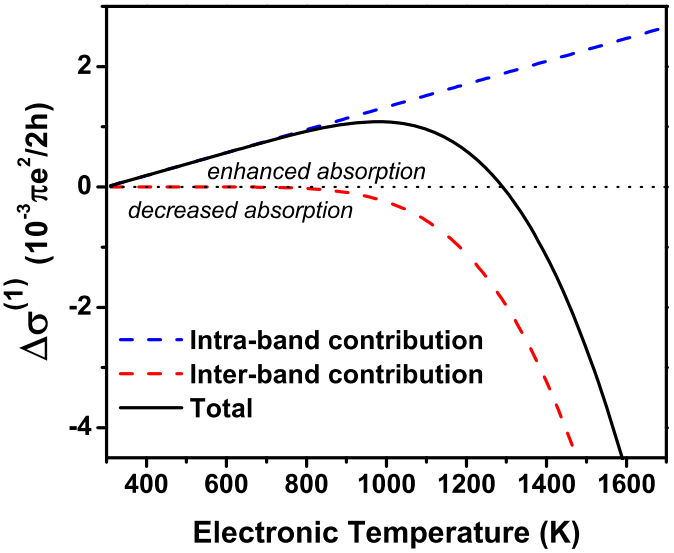

Figure 2. Predicted change in the optical conductivity of graphene as a function of electronic temperature as calculated from equation (1) for $\hbar\omega = 1.55\,\mathrm{eV}$ and a fixed Drude scattering rate of $\Gamma = 30\,\mathrm{meV}$. The dashed blue and red curves show the expected contributions from intra- and inter-band terms, respectively. The black curve is the total response.

the presence of additional free carriers after optical excitation and scales linearly with the electronic temperature T. The inter-band contribution yields a negative transient $\Delta\sigma^{(1)}_{\mathrm{inter}}$, i.e. bleaching of the absorption, from Pauli blocking of the optical transitions at the photon energy $\hbar\omega$. In our regime of $\hbar\omega = 1.55\,\mathrm{eV} \gg k_{\mathrm{B}}T$, the fractional change in the inter-band conductivity is slight and varies approximately exponentially in T. Accordingly, the intra-band contribution dominates at comparatively low electronic temperatures (low fluence), but, as shown in figure 2, is overwhelmed by the inter-band terms as the temperature increases. Thus the transient *increase* in absorption seen in figure 1(a) for low pump fluence reflects the change in *intra-band* optical response. Increasing the temperature of the system, we expect that the transient absorption will change from *increase* to *decreased* absorption as the effect of Pauli blocking of the inter-band transitions begins to dominate. Indeed, as shown in figures 1(b)–(d), the sign of the transient absorption reverses as we increase the pump fluence.

3.2. Model of the transient optical response for graphene

In order to apply the analysis of the graphene optical response presented in equation (1) to our transient absorption experiment, we introduce a simple model to determine the temporal evolution of the electron temperature $T(t)$ induced by the pump laser. As we shall see, this treatment predicts transient optical conductivities compatible both with the low-fluence data already presented and the high-fluence response discussed below. To describe $T(t)$, we first note that on the time scale of our measurement, the deposited energy from the pump pulses rapidly equilibrates among the electronic excitations and the SCOPs [11, 34]. Energy then leaves this coupled subsystem through the anharmonic decay of the SCOPs on a picosecond time scale [37].

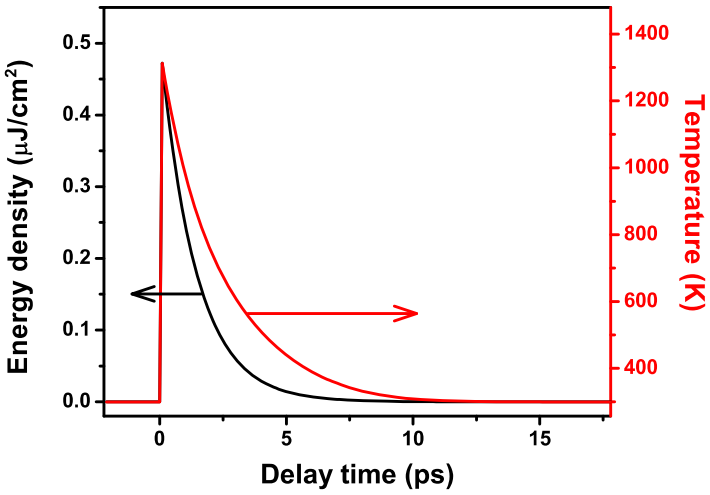

Figure 3. Calculated temporal evolution of the energy density (black) and temperature (red) calculated for the case of an absorbed fluence of 0.5 μJ cm^{-2}. The decay times for the energy density and the temperature are, respectively, 1.4 and 3.1 ps.

To find the resulting electronic temperature $T(t)$, we first consider the heat capacity of the subsystem consisting of the electrons and the SCOPs. Knowledge of this heat capacity allows us to convert the experimental value of the absorbed pump fluence to the temperature of this subsystem. The SCOP excitations are assumed to be in thermal equilibrium with the electronic excitations, as justified by the time scale of the pump pulse. Because of the relatively low heat capacity of the electronic excitations in graphene, the heat capacity is dominated by the SCOPs. Since the SCOPs are the zone-center phonons with energy ~200 meV (Γ-point phonon) and the zone-edge phonons with energy ~150 meV (K-point phonon) [35, 37, 38], we used the Einstein model for heat capacity including these two phonon modes. Therefore, we obtain for the energy density (per unit area) as a function of temperature [39]:

$$u(T) = \frac{A}{(2\pi)^2} f \left[\frac{\hbar\omega_\Gamma}{e^{\frac{\hbar\omega_\Gamma}{k_B T}} - 1} + \frac{\hbar\omega_K}{e^{\frac{\hbar\omega_K}{k_B T}} - 1} \right]. \tag{2}$$

Here A is the area of the Brillouin zone, f is the fraction of Brillouin zone filled by the hot zone-center and zone-edge optical phonons and $\hbar\omega_{\Gamma,K}$ denote, respectively, the Γ- and K-point phonon energies. We determined f (assumed to be temperature independent for simplicity) in equation (2) at a given fluence by comparison with a previous experiment in which transient phonon temperatures for femtosecond laser excitation of graphite were determined by time-resolved Raman scattering [16, 34][6].

To model the temporal evolution of $T(t)$, we assume that the energy stored in the SCOP subsystem (as expressed by equation (2)) relaxes at a rate of $1/\tau_{ph}$ through anharmonic coupling to lower energy phonons [37], with the initial energy density given by the experimental absorbed fluence. The result is shown in figure 3 for a representative absorbed fluence. It is important to

[6] For a temperature range of $500 < T < 2500$ K, the earlier measurements [32] were fit to a polynomial function $F(T) = 1.76 \times 10^{-7} + 1.605 \times 10^{-19}(-4.79 \times 10^{-9}\, T + 4.55 \times 10^{6}\, T^2 + 1484\, T^3 + 0.3225\, T^4)$, where F is the absorbed fluence (or energy density) per graphene layer.

note that because of the nonlinear relationship between the energy density and temperature, the decay time for these two quantities is not the same (figure 3).

Using the calculated temporal evolution of the electronic temperature $T(t)$, we can then predict the transient absorption through equation (1). To match our experimental conditions, we convolute the simulation with a 300 fs Gaussian form with the results shown in figure 1. In fitting our results, we treat the phonon lifetime τ_{ph} and the Drude scattering rate Γ as adjustable parameters. We note that to match the amplitude of equation (1) with the experimental results, we need to include an overall scale factor (kept constant for all pump fluences results). Also, as we discuss below, we use an effective Drude rate Γ that depends on the pump fluence, but is independent of time, to account for the variation of Γ with the temperature of the electrons and SCOPs. This is obviously an approximation, but one that has the merit of allowing analysis of the data without introducing any further assumptions. In fact, the simplified analysis yielded scattering rates quite similar to the maximum value inferred from a model incorporating the theoretically predicted temperature dependence of the scattering rate. This behavior reflects the fact that the optical conductivity transients at early delay times determine in large measure the value of the effective scattering rate.

The measured time evolution of the optical conductivity in figure 1(a) is reproduced well with this model. We use an effective Drude rate of $\Gamma = 27$ meV and a phonon lifetime of $\tau_{ph} = 1.4$ ps. This lifetime differs significantly from the time constant ($\tau_{exp} = 3.1$ ps) of the conductivity transient and reflects the significant temperature dependence of the phonon heat capacity (figure 3). The electronic temperature, which tracks that of the SCOPs and is described by τ_{exp}, falls more slowly than the energy content of the optical phonons, which is characterized by τ_{ph}. The inferred phonon lifetime of $\tau_{ph} = 1.4$ ps lies between that obtained by time-resolved Raman scattering measurements for graphite (2.2 ps) [34] and for graphene (1.2 ps) [25]. We attribute the slightly longer phonon lifetime compared to that measured previously for graphene [25] to the fact that our graphene samples are suspended, thus eliminating possible decay channels involving the generation of surface polar phonons in the substrate [26, 27, 29]. We note that since the electron and the optical phonon subsystems are largely in thermal equilibrium, the deduced phonon lifetime is an intrinsic property of the sample and is independent of probe wavelength. The decay rate of the observed transient in the optical conductivity will, however, depend on the probe wavelength, as is clear from the inter-band term of equation (1).

At higher pump fluences (and, correspondingly, higher electronic temperatures), the optical conductivity is expected to decrease as state filling of the inter-band transitions begins to dominate the transient response (figure 2). The measured conductivity transients at higher pump fluence are shown in figures 1(b)–(d). With increasing pump fluence, the initial response is indeed negative. At later times when the electronic temperature drops, the intra-band contribution becomes dominant and a positive conductivity change is observed.

The experimental data of figures 1(b)–(d) can be fit (red curves) with the same model of the electronic temperature described above, but now with the inclusion of the inter-band optical response of graphene. Our model can then accurately describe the dynamics of the conductivity transients at all fluences (figures 1(a)–(d)). In this fitting process, we use a single, fluence-independent parameter of $\tau_{ph} = 1.4$ ps for the optical phonon lifetime. This parameter reflects the anharmonic decay rate of these optical phonons. It should not change with pump fluence unless the excitation of the resulting phonon decay modes also increases significantly [40], which is not expected in this regime. On the other hand, the fitting procedure implies that the

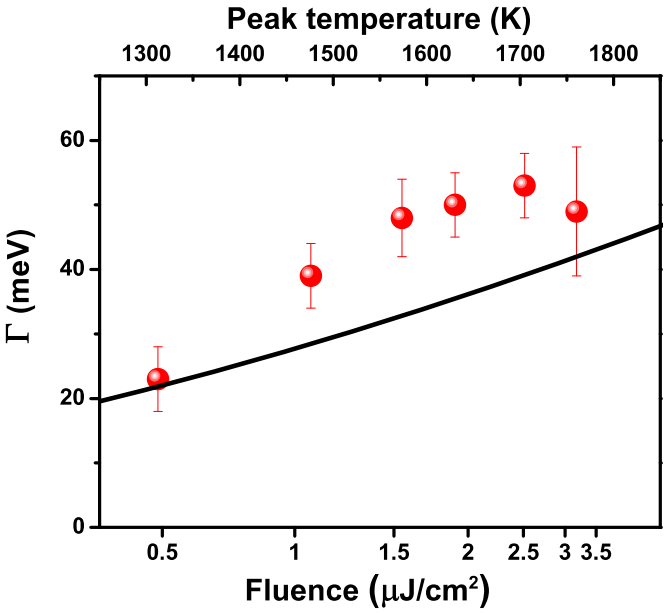

Figure 4. Drude scattering rate Γ (closed circles) as a function of absorbed pump fluence (bottom scale) and of the calculated peak electronic temperature (top scale). The points are inferred from a modeling of the experimental transient optical response of the graphene sample. The black line corresponds to the predicted temperature dependence of Γ arising from electron–optical phonon interactions, as described in the text.

effective Drude rate Γ increases with pump fluence. The inferred variation of Γ is shown in figure 4 as a function of absorbed fluence (bottom scale) and of the peak electronic temperature (top scale) in our model. At high fluence, corresponding to a peak temperature of 1700 K, we find that $\Gamma = 52$ meV. Both this rate and that inferred for lower fluences are higher than the scattering rates implied by conventional transport studies at lower temperatures. Around room temperature, values of Γ in the range of a few meV have been measured [41].

3.3. Calculation of the carrier scattering rate at high temperatures

To understand the origin of the enhanced Drude rate at high temperatures, recall that the SCOPs are high-energy optical phonon modes located at the center and the edge of the Brillouin zone [11, 35, 37]. These phonons are not important for conventional low-bias charge transport measurements at and around room temperature. In this conventional regime, scattering by the emission of such phonons is prohibited because of the low energy of the electrons, while scattering involving phonon absorption is precluded by the very low population of these high-energy phonons. The situation changes when the temperatures of the electrons and the SCOPs become comparable with that of the optical phonons, $\hbar\omega_{\mathrm{ph}}/k_{\mathrm{B}}$ [30, 31]. Electron scattering with such high-energy optical phonons then becomes efficient, leading to a strong temperature dependence of the Drude rate [42]. We expect this scattering process to become the dominant one under conditions of elevated temperature. In keeping with this picture, we present a calculation of the expected temperature dependence of the Drude rate Γ from carrier scattering

with the SCOPs. Without the use of any adjustable parameters, we found, as discussed below, reasonably good agreement with our experimentally inferred scattering rates.

In our calculation, we assume that the two SCOPs are dispersionless with energies of 200 and 150 meV. The self-energy of the electrons in graphene arising from coupling with optical phonons can then be calculated [43] using

$$\Sigma(\vec{k}, \mathrm{i}\omega_n)/\hbar = -\frac{9}{2}\left(\frac{\partial t}{\partial a}\right)^2 \frac{\hbar}{M_c \hbar\omega_{\mathrm{ph}}} \frac{1}{N_c} \sum_{\vec{Q}} \frac{1}{\beta\hbar} \sum_m D^0(\mathrm{i}\nu_m) G^0_{\mathrm{bb}}(\vec{k}-\vec{Q}, \mathrm{i}\omega_n - \mathrm{i}\nu_m). \tag{3}$$

Here $(\partial t/\partial a)$ is the electron–phonon coupling constant as defined in [44], a is the carbon–carbon distance, t is the nearest-neighbor hopping integral in the tight-binding model for graphene, M_c is the mass of a carbon atom and ω_{ph} is the phonon frequency. All other parameters are as defined in [45].

After performing the Matsubara summation, we obtain for the imaginary part of the self-energy

$$\begin{aligned}\Im\Sigma(\vec{k}, \mathrm{i}\omega_n)/\hbar = -\frac{9\pi}{4}\left(\frac{\partial t}{\partial a}\right)^2 \frac{\hbar}{M_c \hbar\omega_{\mathrm{ph}}} \frac{1}{N_c} \sum_{\vec{Q}} &+ \left[n_{\mathrm{B}}(\hbar\omega_{\mathrm{ph}}) + n_{\mathrm{F}}(\varepsilon_{\vec{k}-\vec{Q}})\right] \delta(\varepsilon_{\vec{k}} - \varepsilon_{\vec{k}-\vec{Q}} + \hbar\omega_{\mathrm{ph}}) \\ &+ \left[n_{\mathrm{B}}(\hbar\omega_{\mathrm{ph}}) + 1 - n_{\mathrm{F}}(\varepsilon_{\vec{k}-\vec{Q}})\right] \delta(\varepsilon_{\vec{k}} - \varepsilon_{\vec{k}-\vec{Q}} - \hbar\omega_{\mathrm{ph}}) \\ &+ \left[n_{\mathrm{B}}(\hbar\omega_{\mathrm{ph}}) + n_{\mathrm{F}}(-\varepsilon_{\vec{k}-\vec{Q}})\right] \delta(\varepsilon_{\vec{k}} + \varepsilon_{\vec{k}-\vec{Q}} + \hbar\omega_{\mathrm{ph}}) \\ &+ \left[n_{\mathrm{B}}(\hbar\omega_{\mathrm{ph}}) + 1 - n_{\mathrm{F}}(-\varepsilon_{\vec{k}-\vec{Q}})\right] \delta(\varepsilon_{\vec{k}} + \varepsilon_{\vec{k}-\vec{Q}} - \hbar\omega_{\mathrm{ph}}),\end{aligned} \tag{4}$$

where $\varepsilon_{\vec{k}} = \hbar v_{\mathrm{F}} k$, $v_{\mathrm{F}} = 3ta/2\hbar$, and n_{B} and n_{F} denote, respectively, the Bose–Einstein and Fermi–Dirac distribution functions. The first (last) two terms correspond to intra (inter)-band scattering processes. The scattering rate is obtained from

$$\tau^{-1}_{\vec{k}} = -\Im\Sigma(\vec{k}, \varepsilon_{\vec{k}})/\hbar. \tag{5}$$

To compute $\tau^{-1}_{\vec{k}}$, we need to evaluate the integrals appearing in equation (4). The third integral, however, does not contribute to the scattering rate, since the argument of the δ-function is always positive. We are left with the following integrals:

$$\begin{aligned} I_{\pm} &= \frac{1}{N_c} \sum_{\vec{Q}} \delta(\varepsilon_{\vec{k}} - \varepsilon_{\vec{k}-\vec{Q}} \pm \hbar\omega_{\mathrm{ph}}) \\ &= \frac{a_c}{(2\pi)^2} \int_0^{2\pi} \mathrm{d}\theta \int_0^{Q} Q\,\mathrm{d}Q\,\delta\left(\varepsilon_{\vec{k}} - \sqrt{\varepsilon^2_{\vec{k}} + \varepsilon^2_{\vec{Q}} - 2\varepsilon_{\vec{Q}}\varepsilon_{\vec{k}}\cos\theta} \pm \hbar\omega_{\mathrm{ph}}\right), \\ J_- &= \frac{a_c}{(2\pi)^2} \int_0^{2\pi} \mathrm{d}\theta \int_0^{Q} Q\,\mathrm{d}Q\,\delta\left(\varepsilon_{\vec{k}} + \sqrt{\varepsilon^2_{\vec{k}} + \varepsilon^2_{\vec{Q}} - 2\varepsilon_{\vec{Q}}\varepsilon_{\vec{k}}\cos\theta} - \hbar\omega_{\mathrm{ph}}\right), \end{aligned} \tag{6}$$

where $a_c = 3\sqrt{3}a^2/2$. Energy conservation, as represented by the δ-functions in equation (5), allows us to replace $\varepsilon_{\vec{k}-\vec{Q}}$ in the Fermi–Dirac functions with $\varepsilon_{\vec{k}} \pm \hbar\omega_{\mathrm{ph}}$ for the first and second integrals, and with $\hbar\omega_{\mathrm{ph}} - \varepsilon_{\vec{k}}$ in the fourth one. From the expressions in equation (6), we find

the scattering rate of an electron with momentum $\vec{k}$ within different energy ranges to be for $\varepsilon < \hbar\omega_{\rm ph}$:

$$\tau_\varepsilon^{-1} = C\left[2n_{\rm B}(\hbar\omega_{\rm ph})\hbar\omega_{\rm ph} + (\hbar\omega_{\rm ph} - \varepsilon)\right] + C\hbar\omega_{\rm ph}[n_{\rm F}(\varepsilon + \hbar\omega_{\rm ph}) - n_{\rm F}(\varepsilon - \hbar\omega_{\rm ph})] + C\varepsilon[n_{\rm F}(\varepsilon + \hbar\omega_{\rm ph}) + n_{\rm F}(\varepsilon - \hbar\omega_{\rm ph})], \tag{7}$$

for $\varepsilon > \hbar\omega_{\rm ph}$:

$$\tau_\varepsilon^{-1} = C\left[2n_{\rm B}(\hbar\omega_{\rm ph})\hbar\omega_{\rm ph} + (\varepsilon - \hbar\omega_{\rm ph})\right] + C\hbar\omega_{\rm ph}[n_{\rm F}(\varepsilon + \hbar\omega_{\rm ph}) + n_{\rm F}(\varepsilon - \hbar\omega_{\rm ph})] + C\varepsilon[n_{\rm F}(\varepsilon + \hbar\omega_{\rm ph}) - n_{\rm F}(\varepsilon - \hbar\omega_{\rm ph})]. \tag{8}$$

Here C is defined as

$$C = \frac{3\sqrt{3}}{2}\left(\frac{\partial \ln t}{\partial a}\right)^2 \frac{\hbar}{M_{\rm c}\hbar\omega_{\rm ph}}, \tag{9}$$

where $(\partial t/\partial a)_\Gamma \approx 6.4\,\text{eV Å}^{-1}$ [44] and $(\partial t/\partial a)_K \approx 14\,\text{eV Å}^{-1}$ [45] for zone-center and zone-edge phonons, respectively.

The average electron scattering rate is then determined by [46]

$$\left\langle \tau_\varepsilon^{-1} \right\rangle = \frac{\int \mathrm{d}\varepsilon D(\varepsilon) n_{\rm F}(\varepsilon, T)\tau_\varepsilon^{-1}}{\int \mathrm{d}\varepsilon D(\varepsilon) n_{\rm F}(\varepsilon, T)}, \tag{10}$$

where $D(\varepsilon)$ denotes the density of electronic states of graphene. The resulting Drude scattering rate Γ, shown in figure 4, is obtained by summing up contributions from the two SCOP modes as

$$\Gamma \equiv \hbar\left\langle \tau_\varepsilon^{-1} \right\rangle_\Gamma + \hbar\left\langle \tau_\varepsilon^{-1} \right\rangle_K. \tag{11}$$

As shown in figure 4, the calculated scattering rate Γ increases approximately linearly with temperature T over the relevant range. Comparing this prediction with our experimental results in figure 4, we obtain semi-quantitative agreement of Γ as a function of pump fluence. Better agreement is not anticipated, since the treatment involves several significant simplifications. We first note that the deduced effective Drude scattering rate Γ actually corresponds to fitting the response over a range of electronic temperatures. In our comparison, we have assumed that the result is dominated by the behavior near the peak electronic temperature. More elaborate modeling could take this effect into account. In terms of the underlying description of the optical conductivity at high temperature, our treatment could be improved by a more detailed analysis of the different phonon modes, considered here as two dispersionless branches, involved in the scattering process. More fundamentally, one should also examine possible contributions to Γ from electron–electron scattering processes, which are known to influence the quasi-particles scattering rates [47] and the dc conductivity [48], as well as weaker contributions from acoustic phonons. The absence of these scattering mechanisms in the calculation may account for the predictions of scattering rate lying somewhat below those deduced from the experiment. The analysis is also based on a simple Drude model for the frequency dependence of the intra-band contribution to the optical conductivity. This approximation has not yet been rigorously tested in this limit. Finally, at high electronic temperatures ($T > 1600\,\text{K}$), the experimental values for Γ appear to level off with increasing T. This effect is absent in the model and suggests that screening of the electron–electron and electron–phonon interactions [49, 50] may play a significant role in this regime of high carrier densities.

It is interesting to compare our results with those obtained in high-field dc transport studies. We found that the values for Γ deduced here for high electronic temperatures are also broadly consistent with those obtained in high-field transport measurements in metallic carbon nanotubes at current saturation [30, 31]. In this regime, electron–optical phonon scattering is also considered to be the dominant contribution to Γ. For high-bias transport measurements in graphene [26, 27, 29], the Drude scattering rate is also significantly enhanced compared to the low-field behavior. This effect has, however, been attributed to interaction of the carriers with polar phonons in the substrate on which the graphene is deposited. Our results imply that even for suspended graphene, which lacks these substrate-mediated interactions, the scattering rate will be strongly enhanced at elevated electronic temperatures.

4. Conclusion

We have examined ultrafast carrier dynamics in freely suspended graphene samples by optical pump–probe measurements. A crossover of the transient optical response of graphene from enhanced to decreased optical conductivity is observed with increasing pump fluence. This behavior can be understood as a result of the coexistence of both intra- and inter-band contributions to the optical response of graphene. Analysis of the time evolution of the data implies an optical phonon lifetime of 1.4 ps and significantly enhanced Drude scattering rates at high electronic temperatures. Our experiment also demonstrates the importance of free-carrier absorption in the visible spectral range for graphene under non-equilibrium conditions and opens up new opportunities for probing fundamental charge transport properties of this two-dimensional material purely by means of optical measurements.

Acknowledgments

We thank Dr Y Wu, Dr M Koshino, Dr D Song, and Dr H Yan for fruitful discussions and C H Lui for sample preparation. We acknowledge support from the MURI program of the Air Force Office of Scientific Research (Arlington, VA, USA) and from the National Science Foundation under grant numbers DMR-1124894 and DMR-1106225. AHCN acknowledges partial support from the US DOE under grant no. DE-FG02-08ER46512 and from the Office of Naval Research (ONR) under MURI grant no. N00014-09–1-1063. LM acknowledges support from the Conselho Nacional de Pesquisa (CNPq) program in Brazil.

References

[1] Castro Neto A H, Guinea F, Peres N M R, Novoselov K S and Geim A K 2009 The electronic properties of graphene *Rev. Mod. Phys.* **81** 109

[2] Bonaccorso F, Sun Z, Hasan T and Ferrari A C 2010 Graphene photonics and optoelectronics *Nature Photon.* **4** 611–22

[3] Peres N M R 2010 Colloquium: the transport properties of graphene: an introduction *Rev. Mod. Phys.* **82** 2673–700

[4] Xia F N, Mueller T, Golizadeh-Mojarad R, Freitag M, Lin Y M, Tsang J, Perebeinos V and Avouris P 2009 Photocurrent imaging and efficient photon detection in a graphene transistor *Nano Lett.* **9** 1039–44

[5] Sun Z P, Hasan T, Torrisi F, Popa D, Privitera G, Wang F Q, Bonaccorso F, Basko D M and Ferrari A C 2010 Graphene mode-locked ultrafast laser *ACS Nano* **4** 803–10

[6] Xu X D, Gabor N M, Alden J S, van der Zande A M and McEuen P L 2010 Photo-thermoelectric effect at a graphene interface junction *Nano Lett.* **10** 562–6
[7] Zhang X, Liu M, Yin X B, Ulin-Avila E, Geng B S, Zentgraf T, Ju L and Wang F 2011 A graphene-based broadband optical modulator *Nature* **474** 64–7
[8] Gabor N M, Song J C W, Ma Q, Nair N L, Taychatanapat T, Watanabe K, Taniguchi T, Levitov L S and Jarillo-Herrero P 2011 Hot carrier-assisted intrinsic photoresponse in graphene *Science* **334** 648–52
[9] Yan J, Kim M-H, Elle J A, Sushkov A B, Jenkins G S, Milchberg H M, Fuhrer M S and Drew H D 2012 Dual-gated bilayer graphene hot electron bolometer *Nature Nanotechnol.* **7** 472–8
[10] Sun D, Aivazian G, Jones A M, Ross J S, Yao W, Cobden D and Xu X D 2012 Ultrafast hot-carrier-dominated photocurrent in graphene *Nature Nanotechnol.* **7** 114–8
[11] Kampfrath T, Perfetti L, Schapper F, Frischkorn C and Wolf M 2005 Strongly coupled optical phonons in the ultrafast dynamics of the electronic energy and current relaxation in graphite *Phys. Rev. Lett.* **95** 187403
[12] Breusing M, Ropers C and Elsaesser T 2009 Ultrafast carrier dynamics in graphite *Phys. Rev. Lett.* **102** 086809
[13] George P A, Strait J, Dawlaty J, Shivaraman S, Chandrashekhar M, Rana F and Spencer M G 2008 Ultrafast optical-pump terahertz-probe spectroscopy of the carrier relaxation and recombination dynamics in epitaxial graphene *Nano Lett.* **8** 4248–51
[14] Sun D, Wu Z-K, Divin C, Li X, Berger C, De Heer W, First P and Norris T 2008 Ultrafast relaxation of excited Dirac fermions in epitaxial graphene using optical differential transmission spectroscopy *Phys. Rev. Lett.* **101** 157402
[15] Newson R W, Dean J, Schmidt B and van Driel H M 2009 Ultrafast carrier kinetics in exfoliated graphene and thin graphite films *Opt. Express* **17** 2326–33
[16] Lui C H, Mak K F, Shan J and Heinz T F 2010 Ultrafast photoluminescence from graphene *Phys. Rev. Lett.* **105** 127404
[17] Winzer T, Knorr A and Malic E 2010 Carrier multiplication in graphene *Nano Lett.* **10** 4839–43
[18] Peres N M R, Guinea F and Castro Neto A H 2006 Electronic properties of disordered two-dimensional carbon *Phys. Rev.* B **73** 125411
[19] Falkovsky L A and Varlamov A A 2007 Space–time dispersion of graphene conductivity *Eur. Phys. J.* B **56** 281–4
[20] Mak K F, Sfeir M Y, Wu Y, Lui C H, Misewich J A and Heinz T F 2008 Measurement of the optical conductivity of graphene *Phys. Rev. Lett.* **101** 196405
[21] Geim A K, Nair R R, Blake P, Grigorenko A N, Novoselov K S, Booth T J, Stauber T and Peres N M R 2008 Fine structure constant defines visual transparency of graphene *Science* **320** 1308
[22] Winnerl S *et al* 2011 Carrier relaxation in epitaxial graphene photoexcited near the Dirac point *Phys. Rev. Lett.* **107** 237401
[23] Sensale-Rodriguez B *et al* 2012 Broadband graphene terahertz modulators enabled by intraband transitions *Nature Commun.* **3** 780
[24] Horng J *et al* 2011 Drude conductivity of Dirac fermions in graphene *Phys. Rev.* B **83** 165113
[25] Kang K, Abdula D, Cahill D G and Shim M 2010 Lifetimes of optical phonons in graphene and graphite by time-resolved incoherent anti-Stokes Raman scattering *Phys. Rev.* B **81** 165405
[26] Meric I, Han M Y, Young A F, Ozyilmaz B, Kim P and Shepard K L 2008 Current saturation in zero-bandgap, topgated graphene field-effect transistors *Nature Nanotechnol.* **3** 654–9
[27] Freitag M, Steiner M, Martin Y, Perebeinos V, Chen Z H, Tsang J C and Avouris P 2009 Energy dissipation in graphene field-effect transistors *Nano Lett.* **9** 1883–8
[28] Barreiro A, Lazzeri M, Moser J, Mauri F and Bachtold A 2009 Transport properties of graphene in the high-current limit *Phys. Rev. Lett.* **103** 076601
[29] DaSilva A M, Zou K, Jain J K and Zhu J 2010 Mechanism for current saturation and energy dissipation in graphene transistors *Phys. Rev. Lett.* **104** 236601
[30] Park J Y, Rosenblatt S, Yaish Y, Sazonova V, Ustunel H, Braig S, Arias T A, Brouwer P W and McEuen P L 2004 Electron–phonon scattering in metallic single-walled carbon nanotubes *Nano Lett.* **4** 517–20

[31] Pop E, Mann D, Cao J, Wang Q, Goodson K and Dai H J 2005 Negative differential conductance and hot phonons in suspended nanotube molecular wires *Phys. Rev. Lett.* **95** 155505
[32] Berciaud S, Ryu S, Brus L E and Heinz T F 2009 Probing the intrinsic properties of exfoliated graphene: Raman spectroscopy of free-standing monolayers *Nano Lett.* **9** 346–52
[33] Mak K F, Shan J and Heinz T F 2011 Seeing many-body effects in single- and few-layer graphene: observation of two-dimensional saddle-point excitons *Phys. Rev. Lett.* **106** 046401
[34] Yan H, Song D, Mak K F, Chatzakis I, Maultzsch J and Heinz T F 2009 Time-resolved Raman spectroscopy of optical phonons in graphite: phonon anharmonic coupling and anomalous stiffening *Phys. Rev.* B **80** 121403
[35] Piscanec S, Lazzeri M, Mauri F, Ferrari A C and Robertson J 2004 Kohn anomalies and electron–phonon interactions in graphite *Phys. Rev. Lett.* **93** 185503
[36] Winzer T and Malić M 2012 Impact of Auger processes on carrier dynamics in graphene *Phys. Rev.* B **85** 241404
[37] Bonini N, Lazzeri M, Marzari N and Mauri F 2007 Phonon anharmonicities in graphite and graphene *Phys. Rev. Lett.* **99** 176802
[38] Lazzeri M and Mauri F 2006 Nonadiabatic Kohn anomaly in a doped graphene monolayer *Phys. Rev. Lett.* **97** 266407
[39] Ashcroft N W and Mermin N D 1976 *Solid State Physics* (Toronto: Thomson Learning)
[40] Chatzakis I *et al* 2011 Temperature dependence of the anharmonic decay of optical phonons in carbon nanotubes and graphite *Phys. Rev.* B **83** 205411
[41] Bolotin K I, Sikes K J, Hone J, Stormer H L and Kim P 2008 Temperature-dependent transport in suspended graphene *Phys. Rev. Lett.* **101** 096802
[42] Stauber T, Peres N M R and Castro Neto A H 2008 Conductivity of suspended and non-suspended graphene at finite gate voltage *Phys. Rev.* B **78** 085418
[43] Stauber T, Peres N M R and Guinea F 2007 Electronic transport in graphene: a semiclassical approach including midgap states *Phys. Rev.* B **76** 205423
[44] Neto A H Castro and Guinea F 2007 Electron–phonon coupling and Raman spectroscopy in graphene *Phys. Rev.* B **75** 045404
[45] Lazzeri M, Attaccalite C, Wirtz L and Mauri F 2008 Impact of the electron–electron correlation on phonon dispersion: failure of LDA and GGA DFT functionals in graphene and graphite *Phys. Rev.* B **78** 081406
[46] Harrison P 2005 *Quantum Wells, Wires and Dots: Theoretical and Computational Physics of Semiconductor Nanostructures* (New York: Wiley)
[47] Hwang E H, Hu B Y K and Das Sarma S 2007 Inelastic carrier lifetime in graphene *Phys. Rev.* B **76** 115434
[48] Kozikov A A, Savchenko A K, Narozhny B N and Shytov A V 2010 Electron–electron interactions in the conductivity of graphene *Phys. Rev.* B **82** 075424
[49] Hwang E H and Das Sarma S 2009 Screening-induced temperature-dependent transport in two-dimensional graphene *Phys. Rev.* B **79** 165404
[50] Attaccalite C, Wirtz L, Lazzeri M, Mauri F and Rubio A 2010 Doped graphene as tunable electron–phonon coupling material *Nano Lett.* **10** 1172